

Finite Fracture Mechanics extension to dynamic loading scenarios

*Original*

Finite Fracture Mechanics extension to dynamic loading scenarios / Chao Correas, A., Cornetti, P., Corrado, M., Sapora, A.. - In: INTERNATIONAL JOURNAL OF FRACTURE. - ISSN 0376-9429. - 239:2(2023), pp. 149-165. [10.1007/s10704-022-00655-x]

*Availability:*

This version is available at: 11583/2975238 since: 2023-01-30T09:18:21Z

*Publisher:*

Springer

*Published*

DOI:10.1007/s10704-022-00655-x

*Terms of use:*

This article is made available under terms and conditions as specified in the corresponding bibliographic description in the repository

*Publisher copyright*

(Article begins on next page)



# Finite Fracture Mechanics extension to dynamic loading scenarios

A. Chao Correas · P. Cornetti · M. Corrado · A. Sapora

Received: 4 February 2022 / Accepted: 6 July 2022 / Published online: 6 October 2022  
© The Author(s) 2022

**Abstract** The coupled criterion of Finite Fracture Mechanics (FFM) has already been successfully applied to assess the brittle failure initiation in cracked and notched structures subjected to quasi-static loading conditions. The FFM originality lies in addressing failure onset through the simultaneous fulfilment of a stress requirement and the energy balance, both computed over a finite distance ahead of the stress raiser. Accordingly, this length results to be a structural parameter, thus able to interact with the geometry under investigation. This work aims at extending the FFM failure criterion to dynamic loadings. To this end, the general requisites of a proper dynamic failure criterion are first shortlisted. The novel Dynamic extension of FFM (DFFM) is then put forward assuming the existence of a material time interval that is related to the coalescence period of microcracks upon macroscopic failure. On this basis, the DFFM model is investigated in case a one-to-one relation between the external solicitation and both the dynamic

stress field and energy release rate holds true. Under such a condition, the DFFM is also validated against suitable experimental data on rock materials from the literature and proven to properly catch the increase of the failure load as the loading rate rises, thus proving to be a novel technique suitable for modelling the rate dependence of failure initiation in brittle and quasi-brittle materials.

**Keywords** Dynamic fracture · Finite Fracture Mechanics · Incubation-Time failure criterion · Coalescence period · Loading rate · Rock materials

## 1 Introduction

The extensive development that the fracture mechanics field has undergone in the last years has opened the door to the successful prediction of brittle failure in complex scenarios. In this regard, the Finite Fracture Mechanics (FFM) criterion (Leguillon 2002; Cornetti et al. 2006) stands out for its physical soundness and predictive capability. The approach assumes that crack initiation happens along a finite distance as early as stress and energy necessary conditions are fulfilled. This allows FFM to acquire its most distinctive feature: a non-local definition assessed over a structural distance (identified as the crack initiation length) that does not require ad hoc magnitudes. Likewise,

---

A. Chao Correas (✉) · P. Cornetti ·  
M. Corrado · A. Sapora  
Department of Structural, Geotechnical and Building  
Engineering, Politecnico di Torino, Corso Duca degli  
Abruzzi 24, 10129 Turin, Italy  
e-mail: arturo.chaacorreas@polito.it

A. Chao Correas  
Elasticity and Strength of Materials Group, School of  
Engineering, Universidad de Sevilla, Camino de los  
Descubrimientos S/N, 41092 Seville, Spain

FFM has been proven to yield accurate crack onset predictions in both non-singular and singular structural domains under quasi-static loading regimes, see, for instance, the recent works by Chao Correias et al. (2021) and Doitrand et al. (2021). Noteworthy, a novel study by Doitrand et al. (2022) conducted, via a numerical implementation of FFM, a thorough analysis on the effect that the kinetic energy has in the failure initiation under quasi-static loading regimes.

Nonetheless, the analysis of fracture initiation in the dynamic loading regime is much more complex to handle as of the difficulty in coping with a load varying in time. In this context, different dynamic failure criteria were proposed to extend their static counterparts. The “Classical dynamics approach” (see e.g. Petrov et al. 2003) assumes that two ultimate material properties, namely dynamic strength  $\sigma_{c,dyn}$  and toughness  $K_{Ic,dyn}$ , are rate-dependent material functions obtainable from experiments. On that basis, the Maximum Stress criterion and the Linear Elastic Fracture Mechanics approach get straightforwardly extended to dynamics for plain and cracked geometries, respectively. The simplicity of the criterion makes it readily available for numerical implementation. On the other hand, the local and instantaneous assessment precludes its use for certain cases of interest, e.g. for notches or short pulse loadings, whilst material characterization becomes rather complex. Noteworthy, the well-known Johnson–Cook model for plastic failure (Johnson and Cook 1985) would fall within this criteria category in what concerns the modelling of the strain-rate dependence in the effective strength of elastoplastic materials.

A more robust yet simple approach was introduced by Yin et al. (2015) with the Dynamic reformulation of the Theory of Critical Distances (DTCD). Although still based on material functions for describing the rate dependence of the material’s ultimate properties, a non-local definition analogous to that of TCD (Taylor 2007) was introduced to enable the prediction of failure in notched geometries. Experimental results from dynamic tensile tests of notched metallic specimens were also provided in Yin et al. (2015), and DTCD failure predictions were reported to remain within the  $\pm 20\%$  error range. However, DTCD inherited from its static counterpart the use of a material length for the non-local criterion assessment, precluding its application to small-size specimens, for

instance. Besides, just like in the classical approach, the evaluation of the DTCD condition is instantaneous.

On the contrary, Petrov and Morozov (1994) looked at the dynamic failure initiation problem from a different perspective when proposing the Structural-Time criterion, later renamed as Incubation-Time (IT) criterion (see e.g. Bratov and Petrov 2007). Indeed, the ultimate material properties  $\sigma_c$  and  $K_{Ic}$  are assumed to be independent of the loading (or deformation) rate for materials with negligible viscous effects. The dynamic dependence of failure onset is instead considered to stem from the temporal non-uniformity in the stress field, in the same way its variation along space leads to the size-effect in quasi-static setups. The corresponding dynamic failure condition, constructed upon the Neuber–Novozhilov criterion, has a non-local and non-instantaneous definition: two scalar properties (one length and one time period) are required, along with the static material strength. Noteworthy, the static fracture toughness comes into play through the material length. Consequently, the material’s dynamic characterization results much simpler, and the IT approach can explain phenomena observed in dynamic experiments, e.g. the post-peak failure triggering captured by Homma et al. (1983) for failure under short pulse loadings. IT criterion was proven accurate with respect to experimental results corresponding to different failure problems, *inter alia* crack initiation in pre-cracked geometries (Petrov and Morozov 1994; Petrov and Sitnikova 2004) or spalling (Petrov et al. 2003). On the other hand, the use of a fixed material length still limited the applicability of the IT criterion similarly to DTCD.

In this line, an energy-based counterpart of the IT criterion was introduced by Pugno (2006). Designated as Dynamic Quantized Fracture Mechanics (DQFM) approach, the proposed non-local and non-instantaneous condition for failure is expressed in terms of the dynamic energy release rate and the fracture energy. Akin to the IT, the DQFM approach requires a strength measure of the material (the fracture energy), plus a characteristic length and a time period. Likewise, both IT and DQFM approaches were reported in Pugno (2006) to yield similar dynamic dependence of the failure load for the case of notched metallic specimens under tensile testing. Nonetheless, the DQFM approach also presents disadvantages: for instance, the use of a non-local energy condition for failure

renders it noticeably more complex to implement than its stress counterpart.

Given that there is still room for improvement in what concerns to dynamic failure criteria and provided the good reliability already showcased by the as-now FFM approach, the present study will address its extension to dynamic loading conditions, resulting in the novel Dynamic FFM (DFFM). It should be highlighted that the present work is limited to investigating the dependence of failure onset with the loading rate, being the study of dynamic crack propagation out of scope. Therefore, the term dynamic here does only refer to the rapid nature of the exerted solicitations.

The study is onwards structured in five sections. Section 2 is devoted to the determination of certain general requirements to be fulfilled by dynamic fracture criteria. With those in mind, the DFFM proposal is presented in Sect. 3. Then, the most relevant existent dynamic failure criteria are collected and analyzed in Sect. 4. The particularization of DFFM for two case studies, namely the Semi-Circular Bend (SCB) and the Brazilian Disk (BD) tests, is developed in Sect. 5 along with the comparison with results from suitable dynamic experiments on Laurentian granite (Wu et al. 2015; Yao et al. 2019a, b). Note that the considered geometries are commonly investigated in static setups (Torabi et al. 2017; Doitrand and Sapora 2020; Ghoulou et al. 2021; Sangsefidi et al. 2021). Finally, the conclusions of the study and the outlooks for future developments are given in Sect. 6.

## 2 Requirements for a proper dynamic failure criterion

Let us consider here the generic dynamic loading scenario presented schematically in Fig. 1a: a structural domain  $\Omega$ , filled with a homogeneous, isotropic, brittle, and linear elastic material, that is subjected to a given external loading  $\Sigma_{dyn}(t)$  and to certain boundary conditions. In addition, it is imposed that  $|\Sigma_{dyn}(t)|$  is null for  $t \leq 0$  and nonzero for  $t > 0$ . In such a case, a dynamic stress field  $\sigma_{dyn}(r, t)$  related to the applied  $\Sigma_{dyn}(t)$  can develop within  $\Omega$ . Moreover, this stress field is such that fracture-like failure initiation is expected to take place within a “stationary” localized

region represented by  $\Gamma$ , e.g. a pre-existing stress raiser, and a subsequent crack in the prospective failure plane may be described by a characteristic length  $\Delta$ . The Dynamic Energy Release Rate magnitude  $G_{dyn}(\Delta)$ , also related to  $\Sigma_{dyn}(t)$ , can thus be introduced. Noteworthy, the variation of kinetic energy upon crack propagation is inherently considered within the definition of  $G_{dyn}(\Delta)$  (see Freund 1990).

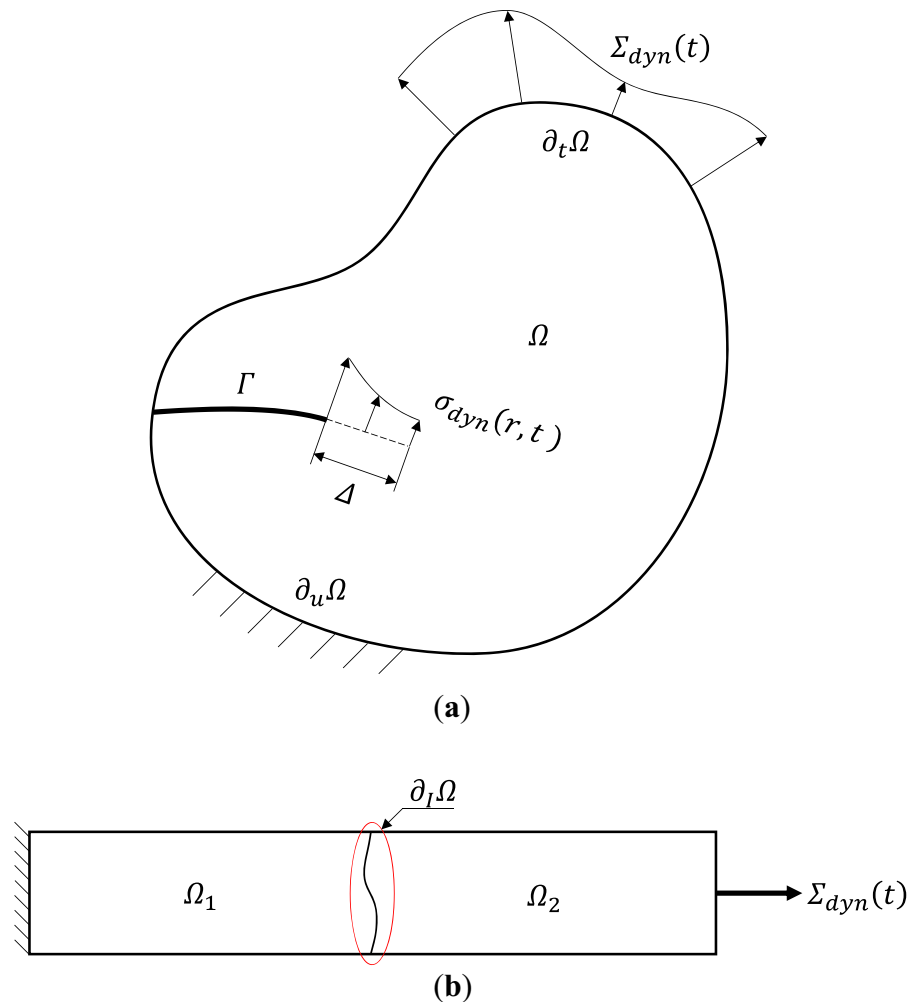
If the external loading presents a slow enough variation over time, i.e.  $\dot{\Sigma}_{dyn} \rightarrow 0$ , the above defined dynamic problem would tend to the particular case of a quasi-static loading scenario, thus implying the first (and most obvious) requirement for a proper dynamic criterion: it should also be applicable to quasi-static loading scenarios. As a result, all the requirements already determined in the literature for static failure criteria should also apply to dynamic ones.

A second requirement arises from the law of conservation of momentum: let us consider, for instance, the domain  $\Omega$  in Fig. 1b. It consists of two rigid subdomains  $\Omega_1$  and  $\Omega_2$ , each one with non-zero mass and in contact through a generic interface ( $\partial_I \Omega$ ), so that no tensile force interaction can be exerted through it. Furthermore,  $\Omega_1$  is fixed, whereas  $\Omega_2$  is subjected to the external dynamic load  $\Sigma_{dyn}(t)$ . Therefore,  $\Omega$  can be supposed to fail should  $\Omega_1$  and  $\Omega_2$  cease to be in contact. Likewise, since no tensile force is transmitted through  $\partial_I \Omega$ , the equivalent strength of  $\Omega$  is null.

The subdomain  $\Omega_2$  should necessarily change its velocity for failure (separation) to take place. And having both subdomains non-zero masses, a change in velocity can only occur when  $\Sigma_{dyn}(t)$ , regardless of its maximum value, generates a non-zero impulse. This proves that for a generic dynamic scenario, any proper failure criterion should be written in terms of impulses instead of forces (or stresses). In this sense, the maximum stress criterion was proven to violate the law of conservation of momentum for short pulses of large amplitude in Petrov et al. (2003).

As a result, the introduction of the impulse among the magnitudes for dynamic failure criterion assessment makes it of non-instantaneous nature. Remarkably, this means that there exists some symmetry between temporal and spatial coordinates: whenever the gradient in the stress field of a domain is non-zero with respect to spatial and/or temporal coordinates,

**Fig. 1** Schematic representation of: **a** a generic structural domain under dynamic load conditions, and **b** the domain used for the proof of the second requirement for a dynamic failure criterion



non-local and/or non-instantaneous failure criteria are needed. Furthermore, the necessity of a non-instantaneous failure criterion is fully supported by the experimental findings from Homma et al. (1983), where it was observed that crack propagation takes place after the instantaneous peak load for short pulse loadings.

Finally, the last requirement to be herein addressed refers to the fulfilment of the conditions on which every failure criterion is based. From a static mindset, their common interpretation is that failure takes place at the minimum load fulfilling the respective condition. However, when considering a generic dynamic loading, this reading should be tempered: material damage is mostly an irreversible phenomenon, thus implying that failure should take place at the first instant – lowest time elapsed from the start of the

loading – in which the criterion is fulfilled. This does not necessarily imply the minimization of the external load at the instant of failure. Nonetheless, these two considerations are equivalent when the external loading  $\Sigma_{dyn}(t)$  is monotonically increasing with time, which is an undercover assumption for all quasi-static setups.

To sum up, the three basic specific requirements to be fulfilled by any proper dynamic failure criterion are:

- (1) It should be applicable for quasi-static scenarios.
- (2) It should be defined in terms of impulses instead of forces or stresses, thus rendering the formulation non-instantaneous.

- (3) The minimization problem through which failure is determined should be expressed in terms of time to fracture.

### 3 Dynamic Finite Fracture Mechanics

In order to account for the requirements shortlisted in the previous section, modifications of the well-established FFM failure criterion are needed for its extension to dynamic scenarios. For the sake of conciseness, the extension will only concern the average stress version of FFM introduced by Cornetti et al. (2006). Subsequently, the herein proposed mathematical definition of the DFFM coupled criterion is shown in Eqs. (1), where it is further assumed, with respect to Sect. 2, that there exists an explicit one-to-one relation between  $\Sigma_{dyn}(t)$  and both  $\sigma_{dyn}$  and  $G_{dyn}$  from which it arises all their temporal dependence.

$$t_f = \min(t \in \mathcal{T}); \quad \Sigma_f = \Sigma_{dyn}(t_f); \quad \Delta_f = \Delta(t_f), \tag{1a}$$

$$\text{where } \mathcal{T} := \left\{ t \mid t : \left[ \int_{A(\Delta)} \sigma_{dyn}(r, \bar{\Sigma}_{dyn}(t)) dA \geq \sigma_c A(\Delta) \right] \right. \tag{1b}$$

$$\left. \int_{A(\Delta)} G_{dyn}(\Delta', \bar{\Sigma}_{dyn}(t)) dA \geq G_c A(\Delta) \right\}. \tag{1c}$$

$$\text{with } \bar{\Sigma}_{dyn}(t) = \frac{1}{\tau} \int_{t-\tau}^t \Sigma_{dyn}(t') dt' \tag{1d}$$

In Eqs. (1), the subindex “*dyn*” emphasizes the dynamic nature of the magnitudes,  $\mathcal{T}$  stands for the set of instants for which both necessary failure conditions, namely Eqs. (1b) and (1c), are met;  $\sigma_c$  and  $G_c$  are, respectively, the static material strength and fracture energy;  $A(\Delta)$  represents the area of a crack whose characteristic length is  $\Delta$  lying in the prospective failure plane, whereas  $\Delta'$  and  $t'$  are dummy integration variables. Likewise, the averaged external solicitation  $\bar{\Sigma}_{dyn}(t)$  defined in Eq. (1d) represents, at each instant  $t$ , a constant-in-time load generating an impulse equal to that of  $\Sigma_{dyn}(t)$  during a period of length  $\tau$  preceding that instant. Mathematically,  $\tau$  can be seen as the minimum time that an external solicitation – constant in time and equal to the failure load of the specimen – must be applied to have crack-like failure. Phenomenologically,  $\tau$  should be regarded as the minimum time required for the microcracks to

coalesce into a single and most energetically convenient macrocrack, and thus will be hereafter called “coalescence period”. However, the DFFM formulation does not interpret  $\tau$  as a lower bound for the time elapsed from the start of the loading to the instant of failure. Indeed, this interval can still span shorter than  $\tau$ , but in said case failure would be expected to not manifest as a single macrocrack, but instead as either multiple cracks or diffused damage developed within the highest tensioned region. Lastly, the failure state is represented by the triad of magnitudes  $\{t_f, \Sigma_f, \Delta_f\}$  that respectively stand for time to failure initiation, (dynamic) failure initiation load and characteristic failure initiation length. As for being the present work only concerned with the study of failure onset, the term “initiation” will be omitted onwards when referring to said magnitudes.

Clearly, the variable subjected to the conditioned minimization in the DFFM approach is time  $t$ , thus

straightforwardly complying with the third requirement set in Sect. 2. Nonetheless, as previously stated, DFFM’s minimization over time corresponds to that over the external solicitation  $\Sigma$  used for FFM under quasi-static assumptions, i.e. when the external solicitation is monotonically “increasing” with time. Furthermore, the equivalence between DFFM and FFM for the quasi-static scenario is also showcased in the conditions for failure, i.e. Eqs. (1b) and (1c), both formulations coinciding when  $\dot{\Sigma} \rightarrow 0$ . This means that Eqs. (1) also comply with the first requirement from Sect. 2.

Finally, the replacement of the instantaneous load  $\Sigma_{dyn}(t)$  with the impulse-based magnitude  $\bar{\Sigma}_{dyn}(t)$  in Eq. (1b) allows for complying with the second requirement, turning the FFM’s force condition into the DFFM’s impulse balance. Likewise, the DFFM’s

energy requirement in Eq. (1c) can be interpreted as follows: macroscopic failure results from the coalescence of microcracks, a cumulative energy-releasing process that develops in a finite time interval, and so, under varying-in-time instantaneous values of the stress and strain fields. Accordingly, the DFFM's energy condition is computed through  $\bar{\Sigma}_{dyn}(t)$  as to catch the effective energy release arising from this coalesce process, in turn assumed to span across a time interval equal to  $\min\{\tau, t_f\}$ . It should be noted that the energy condition shown in Eq. (1c) does not rely on the time integration of the energy release, but instead on the estimation of an effective energy release measure out of the value  $\bar{\Sigma}_{dyn}(t)$ , which in turn is computed through the integral over time of  $\Sigma_{dyn}(t)$  [see Eq. (1d)].

Clearly, the expression in Eqs. (1) can be compactly written as in Eqs. (2) should the respective FFM solution for the quasi-static failure load  $\Sigma_{st,f}$  be known for the analyzed structural system. The coalescence period thus represents the sole property driving the dynamic dependence of failure according to DFFM. Hereafter, it will be assumed that  $\tau$  only depends on the material, although further experimental studies are required to reach any bold statement in this sense.

$$t_f = \min(t \in \mathcal{T}); \Sigma_f = \Sigma_{dyn}(t_f), \quad (2a)$$

$$\text{where } \mathcal{T} := \left\{ \frac{1}{\tau} \int_{t-\tau}^t \Sigma_{dyn}(t') dt' \geq \Sigma_{st,f} \right\}. \quad (2b)$$

To summarize, the proposed DFFM approach is based upon considering failure initiation as not being an instantaneous process, but one that spans over a finite time interval, thus aligning well with the existence of an upper bound for the crack propagation velocity (see Freund 1990). On the other hand, this limitation does not fit well with the conventional FFM approach, where the crack initiation process is assumed instantaneous. Even so, Laschuetza and Seelig (2021) proved that FFM's failure load predictions remain reasonably accurate under quasi-static setups in comparison with numerical CZM results that accounted for inertial effects at a local level. In any case, unleashing the FFM approach from this hypothesis towards rendering it a more complete approach suitable for application to dynamic loading regimes motivated the recent work by Doitrand et al. (2022). Therein, the focus was put on the effect that different

crack velocity profiles – and the associated kinetic energy – have on failure initiation. Likewise, some dynamic effects on failure under both quasi-static and dynamic loadings were addressed. Nonetheless, besides the differences in the scope of each, the approach by Doitrand et al. (2022) is substantially different from DFFM: the former considers failure initiation as a crack propagation event stemming from a stress raiser, whereas the latter assumes it to take place through the energetically convenient coalescence of microcracks.

#### 4 Pre-existing dynamic failure criteria

The main existent failure criteria applicable to the dynamic loading scenarios at hand are now described and put up against the novel DFFM approach proposed in Sect. 3.

The simplest dynamic failure criterion falls under the ‘‘Classical dynamics approach’’ denomination (see Petrov et al. 2003), and it represents the direct dynamic extension of either the Maximum Stress failure criterion or Linear Elastic Fracture Mechanics for non-singular and singular geometries, respectively. Its implementation is based upon comparing, instantaneously and locally, either a relevant component of the stress field or the stress intensity factor with the respective critical values as shown in Eq. (3). In turn, these thresholds present an explicit dependence on the loading (or deformation) rate, being further assumed that the strength and toughness functions are only material dependent and directly derived from experiments.

$$\{\sigma_{dyn}, K_{I,dyn}\}(t_f) = \{\sigma_{c,dyn}, K_{Ic,dyn}\}(\dot{\Sigma}_{dyn}). \quad (3)$$

Notice that the implementation of Eq. (3) first requires to differentiate whether the geometry is singular or not, thus breaching the statement that a proper failure criterion should be straightforwardly applicable to any geometry. In addition, because of its instantaneous and local nature, the criterion is not able to catch neither the post-peak failure observed experimentally in Homma et al. (1983) nor the size-effect of failure in non-singular geometries (see, e.g. Chao Correias et al. 2021). Of course, the largest source of difficulty in applying Eq. (3) arises from the determination of the material functions that determine the

strength and toughness dependence on the loading rate.

On the basis of the approach described by Eq. (3) for capturing the rate dependence of failure, a DTCD set of failure criteria was proposed in Yin et al. (2015) and Alanazi and Susmel (2022). The Line Method version is shown in Eqs. (4), where the rate dependence is solely captured by the variation of both  $\sigma_{c,dyn}$  and  $K_{Ic,dyn}$  (and consequently, of the characteristic length  $L$ ) with the loading rate.

$$\frac{1}{L(\dot{\Sigma}_{dyn})} \int_0^{L(\dot{\Sigma}_{dyn})} \sigma_{dyn}(r, t_f) dr = \sigma_{c,dyn}(\dot{\Sigma}_{dyn}), \quad (4a)$$

$$L(\dot{\Sigma}_{dyn}) = \frac{2}{\pi} \left[ \frac{K_{Ic,dyn}(\dot{\Sigma}_{dyn})}{\sigma_{c,dyn}(\dot{\Sigma}_{dyn})} \right]^2. \quad (4b)$$

Differently from the classical approach, the DTCD criterion presents a non-local definition in terms of stress components, which allows for its use in both notched and unnotched geometries, plus being able to catch the size-effect of failure. Nonetheless, this approach is still instantaneous, it requires the obtention of the strength and toughness rate dependency functions, and it inherits the main limitation of TCD, i.e. the use of a material characteristic length (now dependent on  $\dot{\Sigma}_{dyn}$  through the dynamic strength and toughness) to account for the non-locality. Its implementation for specimens whose size approaches  $L(\dot{\Sigma}_{dyn})$  is thus precluded (see Cornetti et al. 2006).

A radically different method was proposed in Morozov and Petrov (1990) and Petrov and Morozov (1994) with the foundation of the so-called IT failure criterion described in Eqs. (5). Based on the Neuber–Novozhilov force criterion, they considered that the dynamic dependence of the problem is governed by an extra material property  $\tau$ , referred to as incubation time and of simple empirical identification. Note that this latter magnitude is analogous to the coalescence period used in the present DFFM proposal (see Sect. 3). Accordingly, the IT criterion assumes that the dynamic dependence of failure arises from the temporal inhomogeneity of the stress field, in like manner the spatial stress concentration manifests in the failure size-effect. In this sense, the IT approach relies on the material static strength  $\sigma_c$ .

$$\frac{1}{\tau} \int_{t_f-\tau}^{t_f} \frac{1}{d} \int_0^d \sigma_{dyn}(r, t) dr dt = \sigma_c, \quad (5a)$$

$$d = \frac{2}{\pi} \left( \frac{K_{Ic}}{\sigma_c} \right)^2. \quad (5b)$$

The approach in Eqs. (5) describes a non-local and non-instantaneous dynamic failure condition, written in terms of impulses, which does not require empirical rate-dependence functions, although at the cost of adding one extra material property. Indeed, the main drawback of the criterion is that it still relies on a constant characteristic length  $d$  (Eq. (5b)), which reduces its applicability similarly to the DTCD formulation, viz. precluding its use for small-size specimens.

On the other hand, the implementation of energy-based conditions for dynamic failure criteria is limited. One of the few proposals in this direction was undertaken in Pugno (2006) with the so-called DQFM, defined as:

$$\frac{1}{\Delta t} \int_{t_f-\Delta t}^{t_f} \frac{1}{\Delta a} \int_0^{\Delta a} G_{dyn}(a, t) da dt = G_{Ic}, \quad (6)$$

where  $\Delta a$  and  $\Delta t$  were regarded as space and time quanta, respectively.

The parallelism existent between Eqs. (5a) and (6) is clear, although the integration over time of the energy release does not result in a physically sound formulation. Despite this, DQFM agrees with the IT criterion in different aspects, such as the introduction of non-local and non-instantaneous dynamic conditions for failure based on the use of fixed spatiotemporal magnitudes ( $\Delta a - \Delta t$  and  $d - \tau$ ), and the assumption that static strength/toughness measures still hold for failure initiation under dynamic loading.

To summarize, it is clear that DFFM shares many common features with static and dynamic failure criteria from the literature. Just as Cornetti et al. (2006) coupled the Neuber–Novozhilov force criterion with the energy release balance to develop the averaged-stress version of FFM, its dynamic extension – DFFM – is based on coupling a proper energetic balance [see Eq. (1c)] to an impulse-based condition similar to that of the IT criterion in Eq. (5a). Equivalently to what happens in the static case, the coupling of failure conditions allows to define the characteristic length used for the non-locality assessment inherently

within the formulation. Therefore, the increase in complexity of the DFFM formulation is a tradeoff for the enlarged applicability of the method, in turn allowing to sort out the main limitation of the IT criterion while being constructed upon the same foundations, thus being able to mimic its efficacy in a wider range of scenarios.

## 5 DFFM implementation and validation

In order to prove the soundness of the present DFFM approach, its predictions will be compared against the results from dynamic tests available in the literature. In particular, three kinds of stress distributions, namely constant, stress concentration (non-singular field) and stress intensification (singular field) are considered through different specimen geometries (Wu et al. 2015; Yao et al. 2019a, b).

All these experimental results refer to the same material: Laurentian granite, a fine-grained rock that allows using rather small specimens still under the homogeneity assumption. At the same time, it presents quasi-brittle fracture and its behavior can be modelled as linear elastic up to failure (see Iqbal and Mohanty 2006; Chen et al. 2009). Nonetheless, being multi-granular and natural, variability is expected in the mechanical properties, especially in the fracture energy/toughness (Nasseri and Mohanty 2008). In this regard, the determination of the material properties required for the comparison with each set of experiments will be justified in Sect. 5.3.

The dynamic loading conditions for all the considered sets of experiments were imposed by a modified Split-Hopkinson Bar system, which, through the use of the pulse shaping technique, produced loading profiles showcasing an almost constant rate (Frew et al. 2002). This detail results essential for guaranteeing the representativeness of the results, since the loading rate  $\dot{P}$  is, alongside the failure load  $P_f$  and the time to failure  $t_f$ , a magnitude through which the comparison is performed. Mathematically, the exerted load can be accurately modelled by the ramp load:

$$\Sigma_{dyn}(t) = P(t) = \begin{cases} 0 & \text{if } t < 0, \\ \dot{P}t & \text{if } t \geq 0. \end{cases} \quad (7)$$

Additionally, dynamic equilibrium conditions take place in the specimen for the given testing setup (Frew

et al. 2002). This means that the inertial effects are diminished and that static expressions relating the external solicitation  $\Sigma = P$  to both the stress field  $\sigma$  and the stress intensity factor  $K_I$  still hold for such dynamic solicitations  $\Sigma_{dyn}(t) = P(t)$ , as respectively demonstrated in Dai et al. (2008, 2010). Clearly, this simplifies the analytical treatment of the dynamic failure through the DFFM approach, since these expressions are easily achievable from the literature or by Finite Element Analyses (FEAs). It shall be noted that, for dynamic loading conditions and non-propagating cracks, Irwin's relation remains as in the static case (Freund 1990), i.e.  $G_{dyn} = K_{I,dyn}^2/E'$  ( $E' = E$  for plane stress and  $E' = E/(1 - \nu^2)$  for plane strain,  $E$  being the Young's Modulus and  $\nu$  the Poisson's ratio). Thus, the energetic balance in Eq. (1c) can also be written in terms of the dynamic stress intensity factor  $K_{I,dyn}$  and the fracture toughness  $K_{Ic}$ .

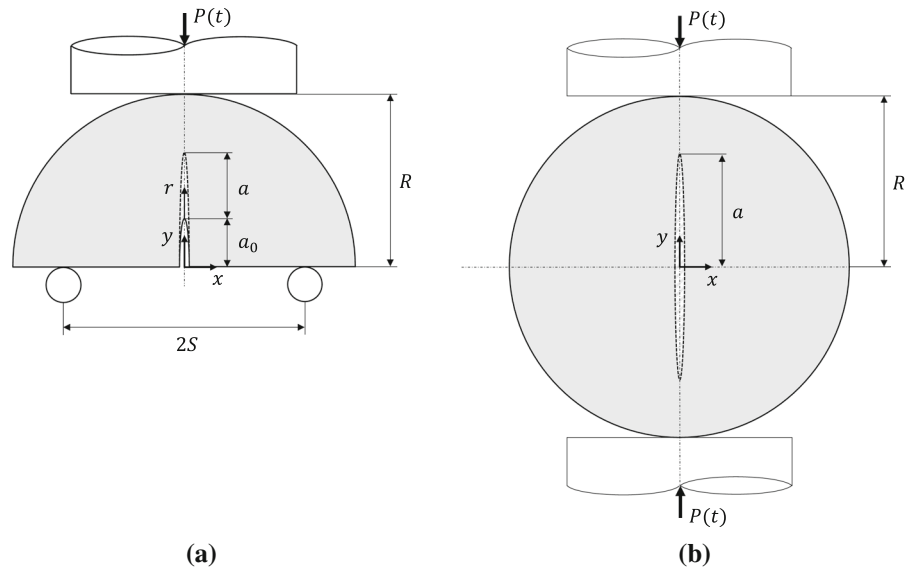
Hereafter, the following subsections will include the proper particularization of the DFFM approach for two different geometries: the SCB and the BD tests, schematically depicted in Fig. 2a and b, respectively. For the former, both Notched (NSCB,  $a_0 > 0$ ,  $a_0$  being the initial length of the sharp notch) and Unnotched (USCB,  $a_0 = 0$ ) configurations will be considered. Then, after careful determination of the material properties, the DFFM's predictions will be compared against experimental results.

### 5.1 SCB geometry

The SCB test is a widespread setup for testing the bending strength of rocks given that specimens can be directly obtained from the cylindrical cores drilled from the mother rock. As seen in Fig. 2a, the geometrical setup of the test is completely defined by four parameters: three describing the specimen shape, i.e. its radius  $R$ , its out-of-plane thickness  $B$  and the length of the initial sharp notch  $a_0$ ; plus the semidistance between rollers  $S$  that defines the boundary conditions. The loading is applied along the midline of the top curved surface through a flat or slightly concave fixture (see Fig. 2a).

For the described setup, expressions for both the stress intensity factor  $K_I$  and the crack opening stress component  $\sigma_{xx}$  can be respectively defined as in Eqs. (8) and (9), where  $F_P$  and  $s_{xx}$  are polynomial

**Fig. 2** Schematic representation of the **a** SCB and **b** BD specimens



shape functions derived numerically from FEAs. Of course, they must be computed for each particular geometry under investigation. Furthermore, note that the stress singularity in the case of  $a_0 > 0$  (NSCB) is

from the dynamic equilibrium conditions, the spatial and temporal problems are uncoupled (and so are their integrals) allowing to perform the variable separation upon system resolution.

$$\left\{ \begin{aligned} & \frac{1}{\Delta_f} \int_0^{\Delta_f} \left\{ \left[ \frac{1}{\tau} \int_{t_f-\tau}^{t_f} P(t) dt \right] \left[ \frac{S_{xx}(r)}{BR} \right] \right\} dr = \sigma_c & (10a) \\ & \frac{1}{\Delta_f} \int_0^{\Delta_f} \left\{ \left[ \frac{1}{\tau} \int_{t_f-\tau}^{t_f} P(t) dt \right]^2 \left[ \pi (a_0 + a) \left( \frac{F_P(a_0 + a)}{BR} \right)^2 \right] \right\} da = K_{Ic}^2 & (10b) \end{aligned} \right.$$

captured by the asymptotic term  $\sqrt{a_0/2r} F_P(a_0)$ , which vanishes when  $a_0 = 0$  (USCB). Additionally, for the NSCB geometry it is ensured that  $s_{xx}(0) = 0$ .

$$K_I(a_0 + a) = \frac{P}{BR} \sqrt{\pi(a_0 + a)} F_P(a_0 + a), \tag{8}$$

$$\sigma_{xx}(r) = \frac{P}{BR} \left[ \sqrt{\frac{a_0}{2r}} F_P(a_0) + s_{xx}(r) \right] = \frac{P}{BR} S_{xx}(r). \tag{9}$$

For a monotonically increasing loading profile  $P(t)$ , the particularization of the DFFM proposal defined in Eqs. (1) results in the system of two nonlinear equations shown in Eqs. (10) as for being the SCB a positive geometry, where  $t_f$  and  $\Delta_f$  represent the unknowns. Noteworthy, per the simplifications arising

Finally, by making use of the ramp loading profile  $P(t)$  defined in Eq. (7), the system of equations governing the DFFM predictions for the failure load  $P_f = \dot{P}t_f$  is obtained. Per the piecewise definition of  $P(t)$ , two scenarios can be met, either the time to fracture  $t_f$  being larger (Regime I) or smaller (Regime II) than  $\tau$ . For the former case, which takes place for low loading rates and whose expression is given in Eqs. (11), the failure load is equal to the static solution plus the linear term  $\dot{P}\tau/2$ . Therefore, the failure load  $P_f$  increases linearly with the loading rate  $\dot{P}$ , whilst the time to fracture  $t_f$  reduces.

$$t_f \geq \tau : \begin{cases} P_f = \frac{\sigma_c BR \Delta_f}{\int_0^{\Delta_f} S_{xx}(r) dr} + \frac{\dot{P}\tau}{2} & (11a) \\ P_f = \frac{K_{lc} BR \sqrt{\Delta_f}}{\sqrt{\pi \int_0^{\Delta_f} (a_0 + a) [F_p(a_0 + a)]^2 da}} + \frac{\dot{P}\tau}{2} & (11b) \end{cases}$$

As  $\dot{P}$  keeps increasing, the failure time yielded by Eqs. (10) eventually reaches the threshold  $\tau$ , thus defining a threshold value for the loading rate  $\dot{P}^*$  that governs the transition from Regime I to Regime II. The latter failure scenario then takes place at high loading rates and its corresponding mathematical expression is given in Eqs. (12). Differently from Regime I, now the dependence of the failure loading with the loading rate is square root-like. Furthermore, both the continuity and smoothness of the failure curves are inherently ensured at the transition point between regimes, i.e. when  $t_f = \tau$

(Eqs. (11) and (12)) to yield the failure load at the given loading rate.

Equations (11) and (12) present the drawback of having  $t_f$  as an output of the problem: thus, one can only know the regime of failure the case under investigation falls within a posteriori. However, this difficulty can be easily overcome by the correspondence in Eq. (14).

$$t_f \leq \tau \iff \dot{P} \geq \frac{2P_{st,f}}{\tau}, \quad (14)$$

$$t_f \leq \tau : \begin{cases} P_f = \frac{\sigma_c BR \Delta_f}{\sqrt{\int_0^{\Delta_f} S_{xx}(r) dr}} \sqrt{2\dot{P}\tau} & (12a) \\ P_f = \frac{K_{lc} BR \sqrt{\Delta_f}}{\sqrt{\pi \int_0^{\Delta_f} (a_0 + a) [F_p(a_0 + a)]^2 da}} \sqrt{2\dot{P}\tau} & (12b) \end{cases}$$

Further analysis of Eqs. (11) and (12) allows stating that, regardless of the failure regime, the characteristic length  $\Delta_f$  results from the solution of Eq. (13).

$$l_{ch} \left[ \int_0^{\Delta_f} S_{xx}(r) dr \right]^2 = \pi \Delta_f \int_0^{\Delta_f} (a_0 + a) F_p^2(a_0 + a) da. \quad (13)$$

Thus, for a given geometry (i.e.  $S_{xx}$  and  $F_p$  fixed),  $\Delta_f$  only depends on Irwin's length, defined as  $l_{ch} = (K_{lc}/\sigma_c)^2$ . This hugely simplifies the establishment of the rate dependence curves of failure. Indeed, for both failure regimes, the solution for  $\Delta_f$  can be directly obtained from Eq. (13) and then inserted into one of the equations of the respective system

where  $P_{st,f}$  represents the static failure load yielded by the average stress version of FFM. Likewise, the rightmost term represents the loading rate threshold  $\dot{P}^*$ .

Thereby, once the static failure load  $P_{st,f}$  is determined, Eq. (14) can be used to determine the failure regime a priori. The introduction of  $P_{st,f}$  in Eqs. (11) and (12) enables considerable simplification of the expressions for the dynamic dependence of the failure load  $P_f$ , resulting in Eqs. (15). Additionally, these equations only depend on the loading profile  $P(t)$  and are thus independent of the geometry under investigation. Likewise, Eqs. (15) also show that  $\Delta_f$  is independent from the loading rate  $\dot{P}$ .

$$P_f = \begin{cases} P_{st,f} + \frac{\dot{P}\tau}{2} & \text{for } \dot{P} \leq \frac{2P_{st,f}}{\tau}, \end{cases} \tag{15a}$$

$$\begin{cases} \sqrt{P_{st,f}}\sqrt{2\dot{P}\tau} & \text{for } \dot{P} \geq \frac{2P_{st,f}}{\tau}. \end{cases} \tag{15b}$$

### 5.2 BD geometry

Although the SCB test generates failure within a tensile region, the non-constant stress profile precludes directly determining the tensile strength out of just its results. For this reason, the constant tensile stress distribution in the failure region characteristic of the BD test makes it suitable for characterizing such a property. The specimen shape can be described by two parameters: the radius  $R$  and the out-of-plane thickness  $B$  (Fig. 2b).

The expression given in Eq. (16) for the crack opening stress component in the BD test keeps valid along the specimen midplane and far enough from the contact points. Being the stress constant, the DFFM’s energy balance does not play any role here, thus simplifying the DFFM particularization. As a result, the expression of the respective stress intensity factor is not required.

$$\sigma_{xx} = \frac{P}{BR} \left( \frac{1}{\pi} \right). \tag{16}$$

Consequently, the particularization of DFFM for the BD test is only governed by the impulse balance from Eq. (1b), which for a monotonically increasing load profile  $P(t)$  particularizes to a single equation with  $t_f$  as the single unknown:

$$\frac{1}{\pi BR} \left( \frac{1}{\tau} \int_{t_f-\tau}^{t_f} P(t)dt \right) = \sigma_c. \tag{17}$$

Finally, by introducing the ramp loading profile described in Eq. (7) into Eq. (17), the failure curves for both failure regimes are respectively obtained as:

$$\dot{P} \leq \frac{2\sigma_c BR\pi}{\tau} : P_f = \sigma_c BR\pi + \frac{\dot{P}\tau}{2}, \tag{18}$$

$$\dot{P} \geq \frac{2\sigma_c BR\pi}{\tau} : P_f = \sqrt{\sigma_c BR\pi} \sqrt{2\dot{P}\tau}. \tag{19}$$

It is clearly seen in Eqs. (18) and (19) that despite the existent differences with respect to the previous experimental setup, the overall behavior of both failure regimes is still governed by the expression in Eqs. (15): Regime I is characterized by the static solution plus the linear term  $\dot{P}\tau/2$ , whilst Regime II presents a square root dependence with the product  $2\dot{P}\tau$ .

### 5.3 Material characterization and comparison with experiments

In order to compare now the DFFM predictions with the experimental results on Laurentian granite, three material properties are required: the strength  $\sigma_c$ , the fracture toughness  $K_{Ic}$ , and the coalescence period  $\tau$ . In this regard, the use of common experimental techniques and material in the dynamic failure experiments on NSCB (Yao et al. 2019b), USCB (Yao et al. 2019a) and BD (Wu et al. 2015) specimens allows for extrapolating certain conclusions from one set of

**Table 1** References, specimen characteristics and material properties used for the comparison of DFFM predictions with experiments

References	Specimen geometry	Dimensions (mm)				Material properties		
		$B$	$R$	$2S$	$a_0$	$\sigma_c$ (MPa)	$K_{Ic}$ (MPa√m)	$\tau$ (μs)
Yao et al. (2019b)	NSCB	25	25	27.5	5	12.8	3.2	69.0
Yao et al. (2019a)	USCB	25	25	27.5	–	12.8	2.9	69.0
Wu et al. (2015)	BD	16	20	–	–	12.8	–	69.0

results to another. The geometrical characteristics of the samples are reported in Table 1. Likewise, being all the specimens under consideration positive geometries, i.e.  $\partial G/\partial a > 0$ , crack onset takes place at the maximum load withstood by the sample, which then undergoes complete failure.

Thereby, since all the experimental comparisons here undertaken refer to the same material, DFFM would ideally correlate the empirical data with identical or at least very similar values for the properties. Nonetheless, the multigranular, heterogeneous and relatively anisotropic internal structure of rocks such as Laurentian granite complicates the energy-releasing mechanism upon failure (see Nasser and Mohanty 2008). This is evident from the variability in the effective fracture toughness measured by different experiments.

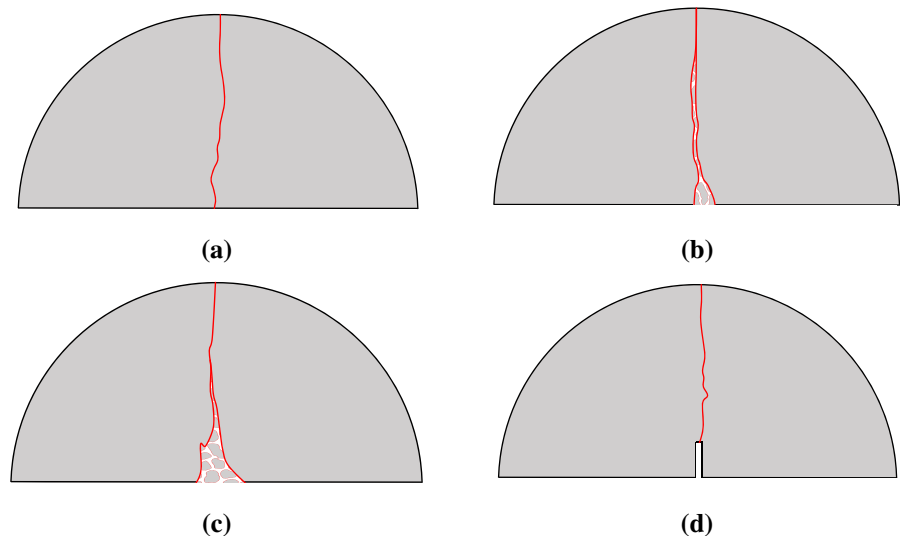
In the present study, the effective value of  $K_{Ic}$  has thus been independently estimated for each specimen type on the basis that the DFFM's static failure load prediction has to match the results yielded by the respective static experiments. However, this choice was not possible for the experimental data set on NSCB tests (Yao et al. 2019b), since no quasi-static tests were therein performed: just for that case,  $K_{Ic}$  was regarded as a best fitting parameter (i.e. its value maximizes the correlation of DFFM predictions with the dynamic empirical data). It should be noted that, once  $\sigma_c$  and  $\tau$  are fixed, a variation in  $K_{Ic}$  results into the vertical shift of the predicted failure curves, with just small changes to their shape. This means that the

interference of the fitting procedure in the representativeness of the comparison results is very limited. The proper calibration of  $K_{Ic}$  for the considered experimental comparisons yields the toughness values shown in Table 1.

On the other hand, due to the concept of tensile strength not being dictated by the energy-releasing mechanism, but instead by the weakest set of the (umpteenth) interfaces within the domain,  $\sigma_c$  may be considered statistically constant for a given material. Thereby, per the constant stress conditions along the failure surface in the BD test,  $\sigma_c$  can be straightforwardly derived from the failure load  $P_f$  obtained in the static performance of such a test through Eq. (18). Experimental results reported in Iqbal and Mohanty (2006) yield the strength value  $\sigma_c = 12.8\text{MPa}$  (see Table 1).

Concurrently, for the proper determination of the coalescence period, its physical meaning must be recalled:  $\tau$  is regarded as the minimum time required for the microcracks lying in the highest loaded region to coalesce into the single macrocrack that releases the most energy. Thereby, its value can only be properly determined from the experimental results in which specimen failure occurs as a fracture-like phenomenon, i.e. along the most energetically convenient surface. For that to happen, either the utmost stressed region within the specimen is highly localized along a surface, e.g. in a singular specimen, so that the microcracks suitable for coalescence are limited to a shallow region; or the loading rate is low enough to

**Fig. 3** Schematic representation of the failure patterns of: **a** USCB with  $t_f = 64.17\mu\text{s}$ , **b** USCB with  $t_f = 40.02\mu\text{s}$ , **c** USCB with  $t_f = 31.74\mu\text{s}$ , and **d** NSCB with  $t_f = 46.23\mu\text{s}$ . Artwork approximately to scale with respect to figures reported in Yao et al. (2019a) for USCBs and Yao et al. (2019b) for NSCBs



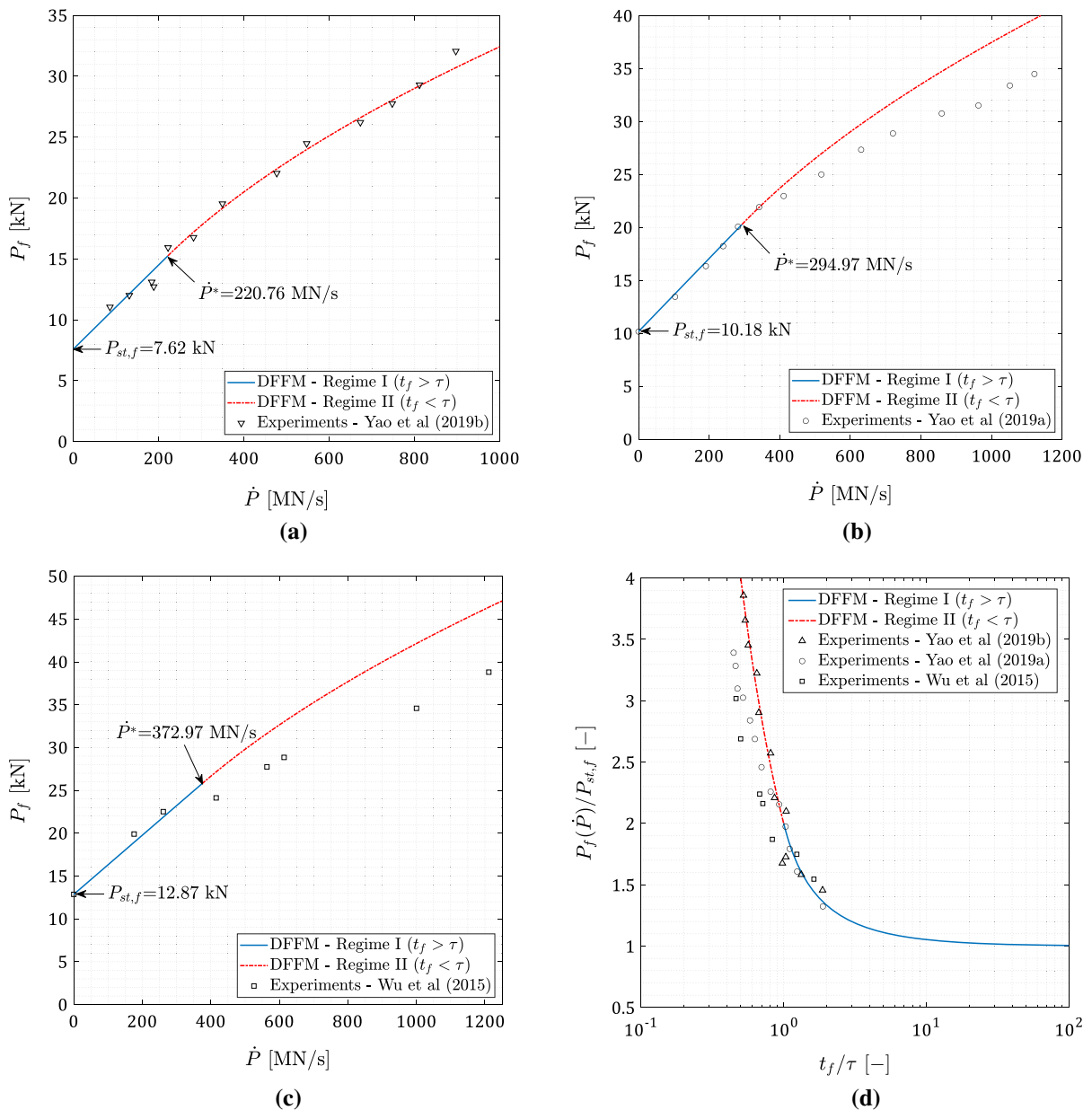


**Fig. 4** Comparison of the DFFM predictions with experimental results in terms of failure load vs loading rate for **a** NSCB specimens (Yao et al. 2019b), **b** USCB specimens (Yao et al.

2019a), **c** BD specimens (Wu et al. 2015), and **d** in terms of strengthening ratio vs. time to fracture for the three considered geometries

yield a time to fracture larger than  $\tau$ . Post-mortem analyses on the failure patterns of USCB and NSCB specimens respectively reported in Yao et al. (2019a, b) and schematized in Fig. 3 support this reasoning. By fitting the proper experimental values, the resultant value for  $\tau$  used for all the subsequently shown comparisons is given in Table 1.

Once the material properties for Laurentian granite have been derived, the attention can be shifted towards analyzing the correlation of the DFFM failure load predictions with the experimental results for varying loading rates. These comparisons are shown in Fig. 4a–c for the dynamic tests performed on NSCB (Yao et al. 2019b), USCB (Yao et al. 2019a) and BD

(Wu et al. 2015) specimens. As per the starting hypotheses upon which the DFFM approach was developed, only the experimental data respective to tests where there is no combination of static and dynamic loadings are considered. Out of these plots, it results evident that for all the three considered experimental setups, DFFM can properly capture the failure behavior within the Regime I, i.e. when  $t_f > \tau$ . Furthermore, the linear trend of the failure load with the loading rate is clearly showcased in all three experimental sets, thus confirming the representativeness of DFFM approach under said dynamic failure regime.

In contrast, the agreement of the DFFM approach with the experimental data within Regime II ( $t_f < \tau$ ) depends on the specimen geometry: it is almost perfect for NSCB tests, whereas there is an overestimation of the failure load for both the USCB and BD tests. Even so, this latter discrepancy, which gradually increases with the loading rate, does not exceed 20% for the considered range of loading rates. The explanation for such a difference can be found in the dependence of the failure patterns on the loading rate reported in the respective references (see, e.g. the schematic representations in Fig. 3). Therein, it was shown that NSCB specimens maintained a fracture-like failure within Regime II, whereas both USCB and BD developed damage-like failure in which the width of the failure initiation region increased with the loading rate. Thereby, for the failure of non-singular specimens under Regime II, there happens an effective increase of energy released per unit of length  $\Delta$  as  $\dot{P}$  grows, thus increasingly affecting the accuracy of the energy balance used for the DFFM approach. Indeed, properly capturing the gradual increase of the energy release per unit of length with  $\dot{P}$  would yield decreasing values for the failure load, thus agreeing better with the experimental results. Consequently, the DFFM overestimation of experimental results can be imputable to the invalidation of the starting hypothesis that enforces failure to occur as fracture-like, which in turn arises from the complex energy-releasing mechanism characteristic of rock materials. It shall be noted that previous studies implementing the FFM approach for rock specimens also found difficulties in determining the fracture toughness so that a proper correlation with the experimental results was obtained, e.g. Leguillon et al. (2007) and Sapora et al. (2022).

Lastly, the effect that the loading rate has on the failure load of all the considered tests is analyzed jointly in Fig. 4d, where the apparent strengthening ratio  $P_f(\dot{P})/P_{st,f}$  is opposed to the time to fracture (normalized by the coalescence period). Clearly, as  $t_f$  increases (and so,  $\dot{P}$  decreases) the failure load tends to its quasistatic solution, i.e.  $P_f(t_f \rightarrow \infty)/P_{st,f} = 1$ . According to Eqs. (15), the DFFM approach yields that the coalescence period is the only parameter governing the dynamic dependence of failure for the studied setups. Therefore, since the same value for  $\tau$  is used in all three considered scenarios, DFFM prediction curves are identical for the three cases and in both failure regimes, i.e.  $t_f > \tau$  and  $t_f < \tau$ . Noteworthy, the diffusive damage showcased by both USCB and BD geometries for failure under Regime II affects both in an analogous fashion.

To conclude, and despite the good predictive capability showcased by the herein proposed DFFM approach, it results natural to wonder how good the rest of theories mentioned in Sect. 4 would perform against these experimental results. Remarkably, IT failure criterion and DFFM yield the exact same prediction for the BD case. For the SCBs instead, the properties in Table 1 would lead to computing the IT's stress integral over a distance  $d$  larger than the specimen itself, thus encountering its main limitation and invalidating the resulting predictions. In what concerns to both the "Classical dynamics approach" and the DTCD, the arbitrariness in defining the strength and toughness dependence with the loading rate renders questionable its implementation. Lastly, the mathematical expressions resulting from the implementation of the DQFM were found to be consistent only for certain combinations of specimen geometry and material: otherwise DQFM delivers complex values for the failure load. Likewise, DQFM's space quantum  $\Delta a$  is often taken equal to  $d$  from Eq. (5b) when macroscopic structures are studied: thereby the validity of its predictions suffers the same drawback than IT's ones should the properties in Table 1 be used.

## 6 Conclusions and future developments

The novel DFFM approach introduced in the present work is the extension of the well-established FFM

static framework to dynamic loading conditions. Based upon considering the failure initiation phenomenon as a process that spans over a material-dependent finite time interval, the FFM stress and energy conditions are modified to comply with the general requisites for dynamic criteria. The resultant coupling of the two non-local and non-instantaneous conditions allows a structure–criterion interplay, rendering the DFFM approach more physically sound than existent dynamic failure criteria, such as the DTCD, IT or DQFM approaches.

The accuracy of the proposed DFFM approach was assessed through the comparison of its failure predictions against experimental results on rocks coming from three different references. These studies were selected since referring to the same experimental technique and material. Additionally, the considered setups allowed to examine the DFFM approach in three different stress distributions: constant profiles, non-singular stress concentrations and singular stress intensifications. The failure predictions yielded by DFFM show overall good agreement with the considered experimental data. Out of its implementation and the correlation with the dynamic empirical results, different conclusions can be drawn:

- The DFFM approach predicts the existence of two differentiated dynamic failure initiation regimes depending on whether the time to failure is larger or smaller than a characteristic time interval (the coalescence period). This is consistent with the findings of dynamic experiments on rocks: for low loading rates (large time to fracture) failure initiates as a single crack, while for high loading rates (small time to fracture) the failure onset region diffuses, and multiple cracks dissipate energy.
- For the cases where the time to fracture is larger than the coalescence period, DFFM is able to perfectly catch the dynamic dependence of the failure load for the three considered geometries. Noteworthy, the trend of the failure load versus the loading rate is linear in this regime.
- At higher loading rates, i.e. time to fracture lower than the coalescence period, the material is not allowed to coalesce the most unfavorable microcracks into a single macrocrack upon failure triggering, resulting in two subcases: for

geometries with highly localized stress raisers, failure initiation can still be modelled as fracture-like and thus DFFM remains accurate; for plain geometries instead, more complex energy-releasing mechanism come into play, turning the crack onset into a damage-like phenomenon and affecting the accuracy of the DFFM approach.

- The joint analysis of all the considered experimental data infers that the coalescence period does not present a strong dependence on the specimen geometry or the pre-propagation stress distribution, and the differences found in the behavior of notched and unnotched samples could be explained in terms of differences in the actual energy-release mechanisms taking place. These findings support the hypothesis of the coalescence period being solely dependent on the material at least for self-similar loading cases.

Despite the good predictive capabilities showcased by the herein proposed DFFM approach, some issues still remain open and require further study. For instance, the formulation is not yet mature enough to properly handle the interaction between static pre-stressing and dynamic loads, being now only applicable to either quasi-static or purely dynamic scenarios. Likewise, the coalescence period should be further characterized for different materials, loading profiles and specimen geometries, towards providing a more complete view on its dependency with the characteristics of the setup.

In this regard, the generalization of the DFFM's conditions for failure should also be addressed so that they still hold in cases where the explicit functions  $\sigma_{dyn}(r, \Sigma_{dyn}(t))$  and  $G_{dyn}(\Delta, \Sigma_{dyn}(t))$  do not exist. For the stress condition, this can be accomplished by replacing Eq. (1b) with the IT condition in Eq. (5a) and substituting the integration over  $d$  by that over  $A(\Delta)$  [see Eq. (20b)]. On the other hand, the equivalent dynamic energy release rate upon which the energy condition in Eq. (1c) is based can be determined (through Irwin's relation) from the temporal averaging of the dynamic stress intensity factor [see Eq. (20c)]. Clearly, Eqs. (1) are recovered from Eqs. (20) when  $\sigma_{dyn}$  and  $K_{I,dyn}$  are proportional to  $\Sigma_{dyn}(t)$ .

$$t_f = \min(t \in \mathcal{T}); \quad \Sigma_f = \Sigma_{dyn}(t_f); \quad \Delta_f = \Delta(t_f), \quad (20a)$$

$$\text{where } \mathcal{T} := \left\{ t \mid t : \left[ \frac{1}{A(\Delta)} \int_{A(\Delta)} \left[ \frac{1}{\tau} \int_{t-\tau}^t \sigma_{dyn}(r, t') dt' \right] dA \geq \sigma_c \right] \right\} \quad (20b)$$

$$\left\{ \left[ \frac{1}{A(\Delta)} \int_{A(\Delta)} \left[ \frac{1}{\tau} \int_{t-\tau}^t K_{I, dyn}(\Delta', t') dt' \right]^2 dA \geq K_{Ic}^2 \right] \right\} \quad (20c)$$

**Acknowledgements** This project has received funding from the European Union's Horizon 2020 Research and Innovation Programme under the Marie Skłodowska Curie Grant Agreement No. 861061.



**Funding** Open access funding provided by Politecnico di Torino within the CRUI-CARE Agreement.

**Open Access** This article is licensed under a Creative Commons Attribution 4.0 International License, which permits use, sharing, adaptation, distribution and reproduction in any medium or format, as long as you give appropriate credit to the original author(s) and the source, provide a link to the Creative Commons licence, and indicate if changes were made. The images or other third party material in this article are included in the article's Creative Commons licence, unless indicated otherwise in a credit line to the material. If material is not included in the article's Creative Commons licence and your intended use is not permitted by statutory regulation or exceeds the permitted use, you will need to obtain permission directly from the copyright holder. To view a copy of this licence, visit <http://creativecommons.org/licenses/by/4.0/>.

## References

- Alanazi N, Susmel L (2022) Theory of Critical Distances and static/dynamic fracture behaviour of un-reinforced concrete: length scale parameters vs. material meso-structural features. *Eng Fract Mech* 261:108220. <https://doi.org/10.1016/j.engfracmech.2021.108220>
- Bratov V, Petrov Y (2007) Application of incubation time approach to simulate dynamic crack propagation. *Int J Fract* 146:53–60. <https://doi.org/10.1007/s10704-007-9135-9>
- Chao Correas A, Corrado M, Sapora A, Cornetti P (2021) Size-effect on the apparent tensile strength of brittle materials with spherical cavities. *Theor Appl Fract Mech* 116:103120. <https://doi.org/10.1016/j.tafmec.2021.103120>
- Chen R, Xia K, Dai F et al (2009) Determination of dynamic fracture parameters using a semi-circular bend technique in split Hopkinson pressure bar testing. *Eng Fract Mech* 76:1268–1276. <https://doi.org/10.1016/j.engfracmech.2009.02.001>
- Cornetti P, Pugno N, Carpinteri A, Taylor D (2006) Finite fracture mechanics: a coupled stress and energy failure criterion. *Eng Fract Mech* 73:2021–2033. <https://doi.org/10.1016/j.engfracmech.2006.03.010>
- Dai F, Xia K, Luo SN (2008) Semicircular bend testing with split Hopkinson pressure bar for measuring dynamic tensile strength of brittle solids. *Rev Sci Instrum* 79:123903. <https://doi.org/10.1063/1.3043420>
- Dai F, Chen R, Xia K (2010) A semi-circular bend technique for determining dynamic fracture toughness. *Exp Mech* 50:783–791. <https://doi.org/10.1007/s11340-009-9273-2>
- Doitrand A, Sapora A (2020) Nonlinear implementation of Finite Fracture Mechanics: a case study on notched Brazilian disk samples. *Int J Nonlinear Mech* 119:103245. <https://doi.org/10.1016/j.ijnonlinmec.2019.103245>
- Doitrand A, Cornetti P, Sapora A, Estevez R (2021) Experimental and theoretical characterization of mixed mode brittle failure from square holes. *Int J Fract* 228:33–43. <https://doi.org/10.1007/s10704-020-00512-9>
- Doitrand A, Molnár G, Leguillon D et al (2022) Dynamic crack initiation assessment with the coupled criterion. *Eur J Mech A/Solids*. <https://doi.org/10.1016/j.euromechsol.2021.104483>
- Freund LB (1990) *Dynamic fracture mechanics*. Cambridge University Press, Cambridge
- Frew DJ, Forrestal MJ, Chen W (2002) Pulse shaping techniques for testing brittle materials with a split Hopkinson pressure bar. *Exp Mech* 42:93–106. <https://doi.org/10.1007/BF02411056>
- Ghoulis S, Bahrami B, Ayatollahi MR et al (2021) Introduction of a scaling factor for fracture toughness measurement of rocks using the semi-circular bend test. *Rock Mech Rock Eng* 54:4041–4058. <https://doi.org/10.1007/s00603-021-02468-1>
- Homma H, Shockey DA, Murayama Y (1983) Response of cracks in structural materials to short pulse loads. *J Mech Phys Solids* 31:261–279. [https://doi.org/10.1016/0022-5096\(83\)90026-1](https://doi.org/10.1016/0022-5096(83)90026-1)

- Iqbal MJ, Mohanty B (2006) Experimental calibration of stress intensity factors of the ISRM suggested cracked Chevron-notched Brazilian disc specimen used for determination of mode-I fracture toughness. *Int J Rock Mech Min Sci* 43:1270–1276. <https://doi.org/10.1016/j.ijrmmms.2006.04.014>
- Johnson GR, Cook WH (1985) Fracture characteristics of three metals subjected to various strains, strain rates, temperatures and pressures. *Eng Fract Mech* 21:31–48. [https://doi.org/10.1016/0013-7944\(85\)90052-9](https://doi.org/10.1016/0013-7944(85)90052-9)
- Laschuetza T, Seelig T (2021) Remarks on dynamic cohesive fracture under static pre-stress—with a comparison to finite fracture mechanics. *Eng Fract Mech* 242:107466. <https://doi.org/10.1016/j.engfracmech.2020.107466>
- Leguillon D (2002) Strength or toughness? A criterion for crack onset at a notch. *Eur J Mech A/Solids* 21:61–72. [https://doi.org/10.1016/S0997-7538\(01\)01184-6](https://doi.org/10.1016/S0997-7538(01)01184-6)
- Leguillon D, Quesada D, Putot C, Martin E (2007) Prediction of crack initiation at blunt notches and cavities—size effects. *Eng Fract Mech* 74:2420–2436. <https://doi.org/10.1016/j.engfracmech.2006.11.008>
- Morozov NF, Petrov YV (1990) Dynamic fracture toughness in crack initiation and propagation problems. *Izv Akad Nauk SSSR MTT (Solid Mech)* 6:108–111 (in Russian)
- Nasseri MHB, Mohanty B (2008) Fracture toughness anisotropy in granitic rocks. *Int J Rock Mech Min Sci* 45:167–193. <https://doi.org/10.1016/j.ijrmmms.2007.04.005>
- Petrov YV, Morozov NF (1994) On the modeling of fracture of brittle solids. *J Appl Mech* 61:710–712. <https://doi.org/10.1115/1.2901518>
- Petrov YV, Sitnikova EV (2004) Dynamic cracking resistance of structural materials predicted from impact fracture of an aircraft alloy. *Tech Phys* 49:57–60. <https://doi.org/10.1134/1.1642679>
- Petrov YV, Morozov NF, Smirnov VI (2003) Structural macromechanics approach in dynamics of fracture. *Fatigue Fract Eng Mater Struct* 26:363–372. <https://doi.org/10.1046/j.1460-2695.2003.00602.x>
- Pugno NM (2006) Dynamic quantized fracture mechanics. *Int J Fract* 140:159–168. <https://doi.org/10.1007/s10704-006-0098-z>
- Sangsefidi M, Akbaridoost J, Zhaleh AR (2021) Assessment of mode I fracture of rock-type sharp V-notched samples considering the size effect. *Theor Appl Fract Mech* 116:103136. <https://doi.org/10.1016/j.tafmec.2021.103136>
- Sapora A, Efremidis G, Cornetti P (2022) Non-local criteria for the borehole problem: Gradient Elasticity versus Finite Fracture Mechanics. *Meccanica* 57:871–883. <https://doi.org/10.1007/s11012-021-01376-6>
- Taylor D (2007) *The theory of critical distances*. Elsevier, Amsterdam
- Torabi AR, Etesam S, Sapora A, Cornetti P (2017) Size effects on brittle fracture of Brazilian disk samples containing a circular hole. *Eng Fract Mech* 186:496–503. <https://doi.org/10.1016/j.engfracmech.2017.11.008>
- Wu B, Chen R, Xia K (2015) Dynamic tensile failure of rocks under static pre-tension. *Int J Rock Mech Min Sci* 80:12–18. <https://doi.org/10.1016/j.ijrmmms.2015.09.003>
- Yao W, Xia K, Jha AK (2019a) Experimental study of dynamic bending failure of Laurentian granite: loading rate and pre-load effects. *Can Geotech J* 56:228–235. <https://doi.org/10.1139/cgj-2017-0707>
- Yao W, Xia K, Zhang T (2019b) Dynamic fracture test of Laurentian granite subjected to hydrostatic pressure. *Exp Mech* 59:245–250. <https://doi.org/10.1007/s11340-018-00437-4>
- Yin T, Tyas A, Plekhov O et al (2015) A novel reformulation of the Theory of Critical Distances to design notched metals against dynamic loading. *Mater Des* 69:197–212. <https://doi.org/10.1016/j.matdes.2014.12.026>

**Publisher's Note** Springer Nature remains neutral with regard to jurisdictional claims in published maps and institutional affiliations.